

PAPER

# General kinetic solution for the Biermann battery with an associated pressure anisotropy generation

To cite this article: K M Schoeffler and L O Silva 2018 *Plasma Phys. Control. Fusion* **60** 014048

View the [article online](#) for updates and enhancements.

## Related content

- [Harmonic effects on ion-bulk waves and simulation of stimulated ion-bulk-wave scattering in CH plasmas](#)  
Q S Feng, C Y Zheng, Z J Liu et al.
- [Kinetic effects in edge plasma: kinetic modeling for edge plasma and detached divertor](#)  
T Takizuka
- [Nonlinear kinetic dynamics of magnetized weibel instability](#)  
L Palodhi, F Califano and F Pegoraro

# General kinetic solution for the Biermann battery with an associated pressure anisotropy generation

K M Schoeffler and L O Silva

GoLP/Instituto de Plasmas e Fusão Nuclear, Instituto Superior Técnico, Universidade de Lisboa, 1049-001 Lisboa, Portugal

E-mail: [kschoeffler@ipfn.ist.utl.pt](mailto:kschoeffler@ipfn.ist.utl.pt)

Received 19 July 2017, revised 16 August 2017

Accepted for publication 24 August 2017

Published 30 November 2017



CrossMark

## Abstract

Fully kinetic analytic calculations of an initially Maxwellian distribution with arbitrary density and temperature gradients exhibit the development of temperature anisotropies and magnetic field growth associated with the Biermann battery. The calculation, performed by taking a small order expansion of the ratio of the Debye length to the gradient scale, predicts anisotropies and magnetic fields as a function of space given an arbitrary temperature and density profile. These predictions are shown to qualitatively match the values measured from particle-in-cell simulations, where the development of the Weibel instability occurs at the same location and with a wavenumber aligned with the predicted temperature anisotropy.

Keywords: kinetic, plasma, astrophysical, laser–plasma interaction, Biermann battery, anisotropy

(Some figures may appear in colour only in the online journal)

## 1. Introduction

Intense magnetic fields generated in laser–solid interaction laboratory experiments [1–5], the seed field required for the generation of astrophysical magnetic fields [6, 7], and experiments that mimic astrophysical events [8–10] have all been attributed to the Biermann battery [11]. The Biermann battery mechanism generates magnetic fields due to misaligned temperature and density gradients. Until recently, the theory behind this mechanism has been restricted to fluid models where an extra non-ideal term is added to Ohm’s law. When modeling the Biermann battery using magnetohydrodynamics, unless the discretization is dealt with carefully, the magnetic fields can grow without bound in a Biermann ‘catastrophe’ [12]. Fluid models in weakly magnetized plasmas typically assume significant collision rates that maintain the pressure tensor in the form of a scalar during relevant time scales<sup>1</sup>. These conditions are often not present in

astrophysical environments and thus a fully kinetic model is necessary.

The Biermann battery has been investigated with fully self-consistent kinetic 3D simulations [13, 14], and recently an analytical model has been presented for the special case with initial density and temperature gradients, which are perpendicular to each other [15]. In this previous paper, the kinetic equivalent of the Biermann battery was demonstrated along with the purely kinetic effect of the generation of a temperature anisotropy in the pressure tensor, where both effects were shown to be relevant for a wide variety of settings including astrophysical shocks and laser experiments with small collision rates. We will hereupon refer to [15] as paper I.

Here, we present a more general model that describes, given an arbitrary density and temperature profile, both the Biermann battery and the evolution of the pressure tensor as a function of time and space. With this description, the Biermann battery can be used to describe many weakly collisional scenarios. Furthermore, the full evolution of the kinetic pressure tensor allows for a measure of the magnitude and direction of the temperature anisotropies again as a function of both time and space. These anisotropies give rise to kinetic

<sup>1</sup> In systems with large magnetic fields (not relevant in this work), where the cyclotron frequency is faster than the collision rate, fluid models with a non-scalar pressure tensor aligned with the field can be formulated [24, 25].

instabilities such as the Weibel instability [16] seen in [13, 14] or instabilities that inhibit the heat flux [17, 18], and thus both this temperature anisotropy and the kinetic Biermann battery are relevant for a wide variety of settings from astrophysical shocks to laser experiments with small collision rates.

## 2. Model

In paper I [15] a few assumptions have been considered to simplify the solution. We show that we can relax some of these assumptions to make the solution general and applicable to many arbitrary systems. First we assumed that the temperature gradient was perpendicular to the density gradient. Second we solved for second order terms, but ignored second order contributions to the initial temperature and density gradients.

Here the time evolution of the distribution function and electromagnetic fields is solved from the coupled Vlasov and Maxwell's equations. We assume that only the electrons play a role and the ions are static, only acting as a neutralizing background, and begin with a instantaneously perturbed Maxwellian electron distribution:

$$f_M = n_0 \left( \frac{1}{2\pi v_{T0}^2} \right)^{3/2} \exp \left( -\frac{1}{2} \frac{v^2}{v_{T0}^2} \right), \quad (1)$$

where the instantaneous perturbation, like in paper I [15], is obtained by replacing  $n_0$  and  $v_{T0}$  with  $n$  and  $v_T$ . However, rather than choosing simple linear and perpendicular gradients, here we examine the most general case, including up to second order gradients with arbitrary angles:

$$n = n_0 \left( 1 + \epsilon x + \frac{1}{2} \epsilon^2 \kappa_{nij} x_i x_j \right), \quad (2)$$

$$v_T = v_{T0} \sqrt{1 + \delta_{\parallel} x + \delta_{\perp} y + \frac{1}{2} \delta^2 \kappa_{Tij} x_i x_j}, \quad (3)$$

$$\epsilon \equiv \frac{\lambda_D}{L_n} \equiv \frac{\lambda_D}{n} \frac{\partial n}{\partial x}(0), \quad \epsilon^2 \kappa_{nij} \equiv \frac{\lambda_D^2}{n} \frac{\partial^2 n}{\partial x_i \partial x_j}(0), \quad (4)$$

$$\delta_{\parallel} \equiv \frac{\lambda_D}{L_{T\parallel}} \equiv \frac{\lambda_D}{T} \frac{\partial T}{\partial x}(0), \quad \delta_{\perp} \equiv \frac{\lambda_D}{L_{T\perp}} \equiv \frac{\lambda_D}{T} \frac{\partial T}{\partial y}(0), \quad (5)$$

$$\delta^2 \kappa_{Tij} \equiv \frac{\lambda_D^2}{T} \frac{\partial^2 T}{\partial x_i \partial x_j}(0). \quad (6)$$

Note that  $\delta$  defined by the gradient scale of the temperature has been divided into two components  $\delta^2 = \delta_{\parallel}^2 + \delta_{\perp}^2$ , corresponding to the gradients parallel and perpendicular to the density gradient.

In this system,  $\mathbf{v}$  is normalized to  $v_{T0}$ ,  $t$  to  $\omega_{pe}^{-1}$ , and  $\mathbf{x}$  to  $\lambda_D$ , where  $\omega_{pe}$  is the plasma frequency for density  $n = n_0$ , and  $\lambda_D \equiv v_{T0}/\omega_{pe}$  is the Debye length. We normalize the fields  $E$  and  $B$  to  $E_0 \equiv m_e v_{T0} \omega_{pe} / e$  and  $B_0 \equiv m_e c \omega_{pe} / e$  respectively. We assume that  $\epsilon$  and  $\delta$  are small and comparable to each other. Furthermore, we take  $\epsilon^2 \kappa_{nij}$  and  $\delta^2 \kappa_{Tij}$  to be comparable to  $\epsilon^2$ .

Assuming  $\mathbf{x} \sim \epsilon^0$ , the initial distribution function to second order in  $\epsilon$  and  $\delta$  is defined in appendix A (equation (39)).

We evolve the Vlasov–Maxwell equations initialized with this distribution function, and either no initial electric or magnetic fields, or natural equilibrium fields that balance the pressure gradient. The steady state electric field for the complete general solution  $E_{st}$  is defined in appendix A (equation (35)).

Note that the perturbation in equation (39) is taken as a given initial state. The Biermann battery is not an instability (in fluid models it grows linearly with time; we show here this remains true in the kinetic case), and therefore it only occurs with non-equilibrium conditions.

The total distribution function evolves as:

$$\frac{\partial f}{\partial t} + \mathbf{v} \cdot \nabla f - (\mathbf{E} + \mathbf{v} \times \mathbf{B}) \cdot \nabla_{\mathbf{v}} f = 0, \quad (7)$$

$$\frac{\partial \mathbf{B}}{\partial t} = -\nabla \times \mathbf{E}, \quad (8)$$

$$\frac{\partial \mathbf{E}}{\partial t} = \int d^3v \mathbf{v} f + \frac{c^2}{v_{T0}^2} \nabla \times \mathbf{B}, \quad (9)$$

where  $\nabla_{\mathbf{v}}$  is the gradient in velocity space, equation (7) is the Vlasov equation, equation (8) is Faraday's law, and equation (9) is Ampere's law. Note that the parameter  $c/v_{T0}$  is written explicitly in terms of the normalization  $v_{T0}$  to emphasize that this is not a universal constant, but a parameter that can vary from system to system.

Following the same assumptions made in paper I [15], we seek solutions to these equations in powers of  $\epsilon$  and  $\delta$ . We assume  $t \sim \mathbf{x} \sim c^2/v_{T0}^2 \sim \epsilon^0 \sim \delta^0$ . Although the solution is only valid when  $\mathbf{x} \sim \epsilon^0$ , at an arbitrary position  $\mathbf{x}$ , the calculation also remains valid with a normalization based on the local  $v_T$  and  $n$ . In some regions where the local  $\epsilon$  and  $\delta$  go to zero, it is the  $\epsilon^2 \kappa_{nij}$  and  $\delta^2 \kappa_{Tij}$  that remain as the small parameters. Besides  $\epsilon$  and  $\delta$ , three other parameters must remain small;  $c_s/v_{T0}$ ,  $v_{T0}^2/c^2$ , and  $\nu/\omega_{pe}$ , where  $c_s$  is the sound speed, and  $\nu$  is the collision frequency. (Again for clarity these parameters are written explicitly with respect to the normalization.) Each of these parameters are assumed to be much smaller than one, but aside from  $\nu/\omega_{pe}$  can in principle remain of order  $\epsilon^0$ . In fact, our calculation assumes  $v_{T0}^2/c^2 \sim \epsilon^0$ , although as long as  $\mathbf{B} \sim \epsilon^2$  (which we find in our solution), it is acceptable for  $v_{T0}^2/c^2 \sim \epsilon^1$ . Small values for these parameters are implicitly assumed when considering static ions, using the non-relativistic Vlasov equation/Maxwellian distribution, and neglecting collisions.

As explained in paper I [15], for the first order solution no magnetic field is generated, and only bulk flows and temperature fluxes could be obtained from the distribution function. It was necessary that we perform our calculation with second order terms ( $\sim \epsilon^2$ ) to see effects including the Biermann battery, and the formation of a temperature anisotropy. Once again it should be emphasized that modifications coming from  $c_s/v_{T0}$  and  $v_{T0}^2/c^2$  can be neglected for both first order and second order solutions, although the terms from the first order solution are then only accurate to  $\epsilon^1$ .

### 3. Density gradient

For the generalized scenario studied here, we first consider the case with only a density gradient ( $\delta = 0$ ). If we assume the initial condition of  $f = f_0$  and no initial electric or magnetic fields, a solution can be found taking an expansion for small  $t$ , restricted to second order in  $\epsilon$ . At this point the only difference from the calculations done in paper I [15] is that we include the second order gradients  $\kappa_{nij}$ .

Following paper I [15], summing over all orders of  $t$  converges to the analytic solution valid for  $t \sim \epsilon^0$ :

$$f = f_0 + \tilde{f}_n, \quad (10)$$

$$\mathbf{E} = \mathbf{E}_{st}[1 - \cos(\omega_{pe,x}t)], \quad (11)$$

where,  $\tilde{f}_n$  is defined in appendix A (equation (40)) and  $\omega_{pe,x} = 1 + \epsilon x/2$  is the plasma frequency based on the  $x$  dependent density,  $n$ . Note that we have made use of the Poincaré–Lindstedt method [19, 20], which by modifying the frequency in the solution, avoids unphysical secularly growing terms. This is done by including additional higher order terms ( $> \epsilon^2$ ) found in the expansion of the sin and cos terms. It is evident that the electric field of this solution oscillates about  $\mathbf{E}_{st}$ .

Despite the use of the Poincaré–Lindstedt technique, there still exists a secular term in  $f$ , which grows linearly with time, and eventually grows beyond  $t = \epsilon^{-1}$ , and breaks the assumptions of the ordering. Thus our model is only valid as long as  $t$  remains small compared to this limit. This term is, however, physical, and represents the increasing electron density associated with the divergence of the electric field:

$$\begin{aligned} \nabla \cdot \mathbf{E} &= (n_i - n_e)/n_0 \\ &= \epsilon^2 \left[ 1 - \cos(\omega_{pe,x}t) - \frac{1}{2}\omega_{pe,x}t \sin(\omega_{pe,x}t) \right]. \end{aligned} \quad (12)$$

The space dependent frequency,  $\omega_{pe,x}$ , gives rise to increasingly shorter scale variations along  $x$  in the electric field, and thus an increasingly large divergence. These variations along  $x$  lead to phase mixing in space and then Landau damping. This damping at early times is exponentially repressed, and does not show up in our expansion. However, when the damping becomes most significant at  $k\lambda_D \sim 1$  (equivalent to  $t \sim \epsilon^{-1}$ ) the assumptions break down. Eventually Landau damping eliminates both the oscillations and the secular term, and thus the electric field should naturally settle to equation (35). If we take equation (35) as the initial condition for the electric field, we arrive at a simple equilibrium solution to equations (7)–(9) where  $\mathbf{E} = \mathbf{E}_{st}$  and  $f = f_0$  both of which do not change with time.

### 4. Temperature gradient

We now consider a second case, with only a temperature gradient ( $\epsilon = 0, \delta \neq 0$ ). For simplicity, at this point we will move to a reference frame where  $\delta_{\parallel} = \delta$ , and  $\delta_{\perp} = 0$ . In this reference frame aligned with the temperature gradient,

$$\delta x' = \delta_{\parallel} x + \delta_{\perp} y \quad (13)$$

and

$$\delta v'_x = \delta_{\parallel} v_x + \delta_{\perp} v_y. \quad (14)$$

Note that when looking at only a temperature gradient we are free to use this reference frame; however, when combining both gradients it is important to return to the original coordinates, replacing  $x'$  and  $v'_x$  with equations (13) and (14).

If we again start with the initial conditions,  $f = f_0$ , and no initial electric or magnetic fields, the solution to equations (7)–(9) is, to second order in  $\delta$ , the following:

$$f = f_{\nabla T} + \tilde{f}_T, \quad (15)$$

$$\mathbf{E} = \mathbf{E}_{st}[1 - \cos(\omega_{pe,x}t)], \quad (16)$$

where  $f_{\nabla T}$  (equation (38)) and  $\tilde{f}_T$  (equation (41)) are defined in appendix A.

Although in principle there is nothing to damp these oscillations, if it were a system with density gradients it would Landau damp as described earlier, and in paper I [15]. As before, we consider equation (35) as the initial condition. This yields a simpler solution where the electric field is constant with time, but it still allows the distribution function to evolve with time as  $f = f_{\nabla T}$ .

Like the scenario with a density gradient, there are terms proportional to  $t$  in the distribution function  $f_{\nabla T}$ , which eventually break the assumptions of the ordering. The second term on the rhs of equation (38) in appendix A is associated with the heat flux, and matches the collisional solution shown in [17] once  $t$  reaches the collision time, unless this term breaks the assumptions of the ordering first, once  $\omega_{pe} = \delta^{-1}$ . If we integrate over  $1, v_i$ , and  $v_i v_j$ , we find the density remains  $n$ , and the flow remains 0, but the pressure tensor changes.

In paper I [15], an anisotropy in the pressure tensor which was hotter in the direction of the temperature gradient ( $T'_{xx} > T'_{yy}$ ) was shown to grow proportional to  $\delta^2 t^2$ , and so the temperature gradient naturally lead to a temperature anisotropy, which gives rise to kinetic instabilities such as the Weibel instability [16] seen in [13] or can drive instabilities that inhibit the heat flux [17, 18]. Again we define the temperature tensor as:

$$T_{ij} \equiv \frac{1}{n} \int dv^3 v_i v_j f, \quad (17)$$

which is related to the pressure tensor by  $P_{ij} = nT_{ij}$ , and normalized to  $m_e v_{T0}^2$ . The temperature tensor (in the temperature gradient aligned frame) is obtained by substituting  $f_{\nabla T}$  (equation (38)) into equation (17):

$$T_{ij} = v_T^2 \mathbb{I} + T_{\nabla T, ij}, \quad (18)$$

where the change in the temperature due to the temperature gradient is defined as:

$$T'_{\nabla T, ij} \equiv \frac{1}{2} \delta^2 (\omega_{pe,x}t)^2 \left[ \begin{pmatrix} 3 & 0 & 0 \\ 0 & 1 & 0 \\ 0 & 0 & 1 \end{pmatrix} + 2\kappa_{Tij} + \text{Tr}(\kappa_{Tij})\mathbb{I} \right]. \quad (19)$$

Note that the primed notation indicates that this tensor is presented in the temperature gradient aligned frame. Before

doing further analysis on this anisotropic pressure tensor, we will also look into the effects of both  $\epsilon$  and  $\delta$ .

## 5. Biermann battery

We now consider a third case, with both gradients ( $\epsilon \neq 0$ ,  $\delta \neq 0$ ). If we again start with the initial conditions,  $f = f_0$ , and no initial electric or magnetic fields, to second order in  $\delta$  and  $\epsilon$ , the solution to equations (7)–(9) is the following:

$$f = f_{\nabla n, \nabla T} + \tilde{f}_n + \tilde{f}_T + \tilde{f}_{n,T}, \quad (20)$$

$$\mathbf{E} = \mathbf{E}_{st}[1 - \cos(\omega_{pe,x}t)] \quad (21)$$

$$\mathbf{B} = -\epsilon\delta_{\perp}[\omega_{pe,x}t - \sin(\omega_{pe,x}t)]\hat{\mathbf{z}}, \quad (22)$$

where,  $f_{\nabla n, \nabla T}$  (equation (37)) and  $\tilde{f}_{n,T}$  (equation (42)) are defined in appendix A.

Once again the solution oscillates at  $\omega_{pe}$  time scales around a steady state.

Starting with the steady state electric fields, equation (35), we arrive at:

$$f = f_{\nabla n, \nabla T}, \quad (23)$$

$$\mathbf{E} = \mathbf{E}_{st}, \quad (24)$$

$$\mathbf{B} = -\epsilon\delta_{\perp}\omega_{pe,x}t\hat{\mathbf{z}}. \quad (25)$$

We thus see a kinetic solution of the growth of magnetic fields via the Biermann battery, which grows linearly with time and proportional to the cross product between the density and temperature gradients (see equation (25)), confirming the fluid model prediction.

If we substitute  $f_{\nabla n, \nabla T}$  (equation (37)) into equation (17), we find the temperature tensor is modified by an additional term:

$$T_{\nabla n \nabla T, ij} = \frac{1}{2}\epsilon(\omega_{pe,x}t)^2 \begin{pmatrix} \delta_{\parallel} & \delta_{\perp} & 0 \\ \delta_{\perp} & 3\delta_{\parallel} & 0 \\ 0 & 0 & \delta_{\parallel} \end{pmatrix}. \quad (26)$$

If we rotate this into the temperature gradient aligned frame (again indicated by the primed notation), in order to compare with equation (19), it makes more sense to employ  $\epsilon_{\parallel} = \epsilon\delta_{\parallel}/\delta$ , and  $\epsilon_{\perp} = -\epsilon\delta_{\perp}/\delta$ , such that

$$T'_{\nabla n \nabla T, ij} = \frac{1}{2}\delta(\omega_{pe,x}t)^2 \begin{pmatrix} 3\epsilon_{\parallel} & \epsilon_{\perp} & 0 \\ \epsilon_{\perp} & \epsilon_{\parallel} & 0 \\ 0 & 0 & \epsilon_{\parallel} \end{pmatrix}. \quad (27)$$

The full temperature tensor is now given by:

$$T_{ij} = v_T^2 \mathbb{I} + T_{\nabla T, ij} + T_{\nabla n \nabla T, ij}, \quad (28)$$

If we diagonalize the in-plane components (plane including  $\nabla n$  and  $\nabla T$ ) of the matrix from equation (28), the diagonal terms are:

$$\begin{aligned} T''_{xx} &= v_T^2 + \Delta T_0 + \frac{1}{2}A_0, \\ T''_{yy} &= v_T^2 + \Delta T_0 - \frac{1}{2}A_0, \\ T''_{zz} &= v_T^2 + \Delta T_0 - \frac{1}{2}\Delta T_0, \end{aligned} \quad (29)$$

where  $T''_{xx}$  is the hotter direction,  $T''_{yy}$  is the cooler direction,  $\Delta T_0$  is the average increase of these two in-plane components of the temperature, and  $A_0$  is the in-plane temperature anisotropy. For a 2D system where the derivatives in the  $\hat{\mathbf{z}}$  direction are zero the in-plane temperature and anisotropy can be expressed as:

$$\Delta T_0 = (\delta^2 + \delta^2(\kappa'_{Txx} + \kappa'_{Tyy}) + \epsilon_{\parallel}\delta)(\omega_{pe,x}t)^2, \quad (30)$$

$$\begin{aligned} A_0 &= [(\delta^2 + \delta^2(\kappa'_{Txx} - \kappa'_{Tyy}) + \epsilon_{\parallel}\delta)^2 \\ &\quad + (2\delta^2\kappa'_{Txy} + \epsilon_{\perp}\delta)^2]^{1/2}(\omega_{pe,x}t)^2. \end{aligned} \quad (31)$$

(Note that  $A_0$  is equivalent to the anisotropy  $A$  defined in appendix C using the temperature tensor from equation (28).) As long as  $\Delta T_0 < A_0$ ,  $A_0$  is the dominant anisotropy. One can observe that this anisotropy is proportional to the sum of 3 vectors,

$$A_0 = \delta|\delta + \epsilon + \delta\Delta|(\omega_{pe,x}t)^2, \quad (32)$$

where  $\epsilon = \nabla n/n$ ,  $\delta = \nabla T/T$ , and  $\Delta$  is a vector with magnitude  $\Delta = ((\kappa'_{Txx} - \kappa'_{Tyy})^2 + 4\kappa'^2_{Txy})^{1/2}$ , where the components parallel and perpendicular to the temperature gradient are  $\Delta_{\parallel} = (\kappa'_{Txx} - \kappa'_{Tyy})$ , and  $\Delta_{\perp} = 2\kappa'_{Txy}$ . The angle with respect to the temperature gradient, at which the temperature is the largest, can be expressed as:

$$\theta' = \frac{1}{2} \tan^{-1} \left( \frac{\epsilon_{\perp} + \delta\Delta_{\perp}}{\delta + \delta\Delta_{\parallel} + \epsilon_{\parallel}} \right) + \frac{\pi}{2}(1 - \Theta(\delta + \delta\Delta_{\parallel} + \epsilon_{\parallel})), \quad (33)$$

where  $\Theta(x)$  is the step function. Although the first term in equation (33) is restricted to  $-\pi/4 < \theta' < \pi/4$ , the direction of the hotter temperature shifts by  $\pi/2$  when the denominator changes sign (i.e. the temperature aligned with the temperature gradient is cooler). Note that the temperatures parallel or anti-parallel to the temperature gradient are equivalent, so it is justified that  $\theta'$  remains restricted between  $-\pi/4 < \theta' < 3\pi/4$ . We thus have all the information required to take an arbitrary initial distribution of temperature and density gradients, and solve for the time evolution of the temperature, anisotropy, and angle of anisotropy.

Note that the solution is also valid for an arbitrary uniform magnetic field as long as  $\epsilon$ ,  $\delta$ , and  $\Delta$  are all parallel to the magnetic field. The generation of this anisotropy will thus also occur in magnetized plasmas, where different instabilities, such as the firehose instability [21], would likely form.

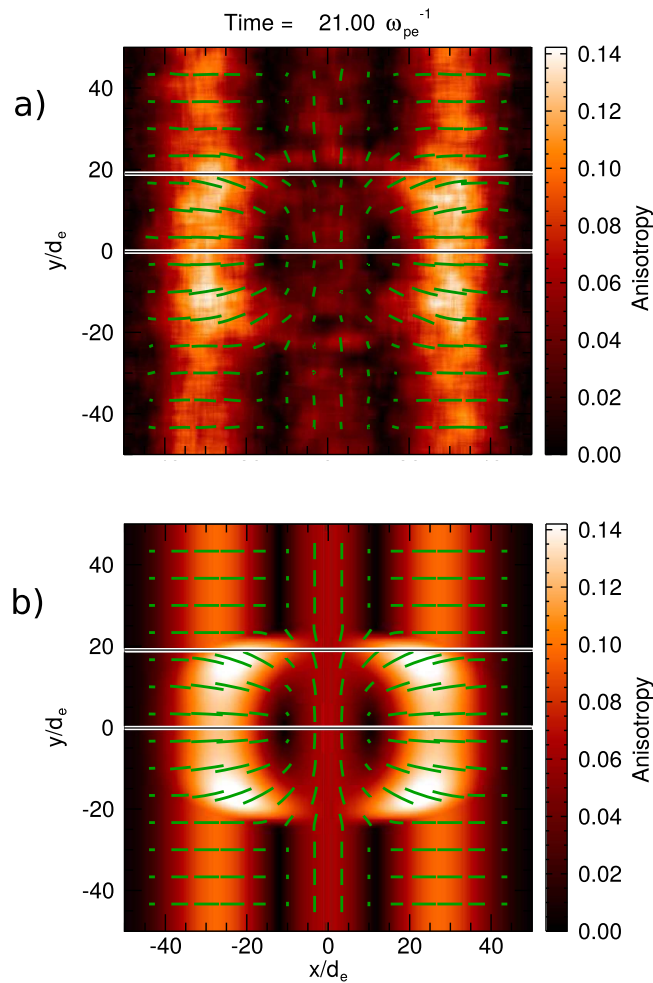


**Figure 1.** Temperature anisotropy measured from PIC simulation given by equations (56)–(57) (a) with  $L_T/d_e = 50$  ( $L_T/\lambda_D = 250$ ) and  $m_i/m_e = 2000$ , at  $\omega_{pe}t = 21$ , from the simulation reported in [14]. The green lines represent the direction ( $i$ ) where the temperature ( $T_{ii}$ ) is maximized. The predicted anisotropy (b) given by equations (31)–(33) for the initial density and temperature distribution from equation (58) show qualitatively similar results. The solid lines represent the location of the line-outs presented in figure 2.

## 6. Numerical simulations

A prediction of the anisotropy and Biermann fields generated at early times ( $t \ll \delta^{-1}$ ), can be obtained via equations (31)–(33) and equation (25). The prediction can be compared directly with particle-in-cell (PIC) simulations using the OSIRIS framework [22, 23], with the aid of a new diagnostic of the temperature tensor. We will thus compare two PIC simulations with this prediction; one with  $L_T/d_e = 50$  ( $L_T/\lambda_D = 250$ ) and  $m_i/m_e = 2000$ , reported in [14], and one based on simulations from [13] ( $L_T/d_e = 200$  ( $L_T/\lambda_D = 1000$ ) and  $m_i/m_e = 25$ ), but where we isolate the magnetic fields due to the Weibel instability by choosing parallel density and temperature gradients both in the radial direction.

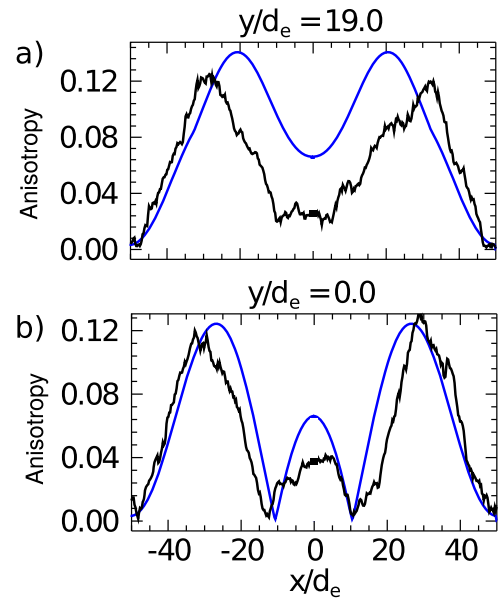


**Figure 2.** Line-outs of the plots of the anisotropy, shown in figure 1 at  $y/d_e =$  (a) 19, and (b) 0. The black curve is the simulation results given by equation (52) (figure 1(a)); the blue is the theoretical predictions assuming the initial density and temperature distribution given by equations (31) and (32) (figure 1(b)).

In figure 1(a), the anisotropy for the simulation with  $L_T/d_e = 50$ , at  $\omega_{pe}t = 21$  is shown. The anisotropy is calculated from the temperature tensor using the expression given by equations (31)–(33) in appendix C. For this simulation,  $\delta^{-1} \approx 250$  based on  $L_T$  and the central density and temperature ( $v_{T0}/c = 0.2$ ). Since  $\omega_{pe}t \ll \delta^{-1}$ , in principle our assumptions are not largely broken. We solve for the small parameters defined in equations (4)–(6) as a function of space using the initial density and temperature distribution from the simulation (shown in appendix D). Note that equations (4)–(6) assume a frame aligned with the temperature gradient. In appendix B, the transformations from an arbitrary frame are shown for reference.

We find that the minimum  $\delta^{-1} \approx 26$ ,  $\epsilon^{-1} \approx 11$ , and  $|\delta^2 \kappa_{ij}|^{-1/2} \approx 26$ , so in certain regions our assumptions are only marginally held. For example in the most extreme case, by  $\omega_{pe}t = 21$  the local value of  $\omega_{pe}t\epsilon \approx 0.75$  (at  $x/d_e \approx 0$ ,  $|y|/d_e \approx 20$ ).

Figure 1(b) shows the theoretically predicted spatial distribution of anisotropy. Despite the marginal assumptions, the distribution matches qualitatively quite well with the simulation results, with only slight differences. The anisotropy around  $|x|/d_e = 30$  expands outward slightly, while the anisotropy growth around  $x/d_e = 0$  is a bit suppressed during this expansion.

In order to get a more quantitative comparison, two cuts of the anisotropy at  $y/d_e = 0$  and 19 are shown in figure 2. The black curve is the simulation, while the blue curve is the prediction for the initial simulation temperature and density profile given in equation (58). The predictions hold very well, with only a slight departure near the region in the center, and a remarkable quantitative agreement on the anisotropy.

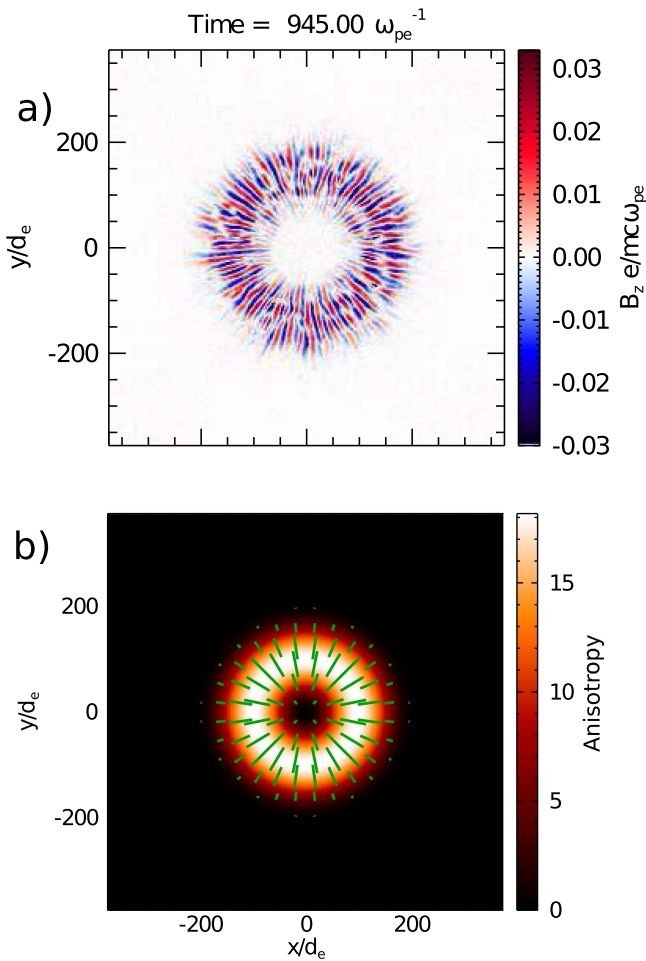


**Figure 3.** Out-of-plane magnetic field  $B_z$  generated by the Weibel instability from the PIC simulation (a) based on simulations reported in [13] ( $L_T/d_e = 200$  ( $L_T/\lambda_D = 1000$ ),  $m_i/m_e = 25$ , at  $t = 945\omega_{pe}^{-1}$ ), isolating the Weibel instability with radially parallel temperature and density gradients. The predicted temperature anisotropy and angle (b) given by equations (31)–(33) for the initial density and temperature distribution from equation (58) coincides with the region where the Weibel instability occurs. The green lines represent the direction ( $i$ ) where the temperature ( $T_{ii}$ ) is maximized.

For the simulation where we isolate the Weibel instability (based on simulations from [13] with  $L_T/d_e = 200$  ( $L_T/\lambda_D = 1000$ ) and  $m_i/m_e = 25$ ), by choosing parallel density and temperature gradients,  $L_n = L_T$  and the temperature proportional to  $r = \sqrt{x^2 + y^2}$  instead of  $x$ . The anisotropy is predicted to point radially outward, and thus only an out-of-plane Weibel magnetic field ( $B_z$ ) should grow with a wavenumber  $k$  in the azimuthal direction. In figure 3(a), the magnetic fields generated by the Weibel instability are shown. Again we show the predicted anisotropy for the initial density and temperature distribution from equation (58). As expected, the Weibel instability coincides with these predicted anisotropy distributions that drive it. Note that the Weibel instability occurs at a slightly larger radius as the anisotropy expands with time.

Finally, in figure 4(a), the magnetic field is shown from the simulation also shown in figure 1. This out-of-plane

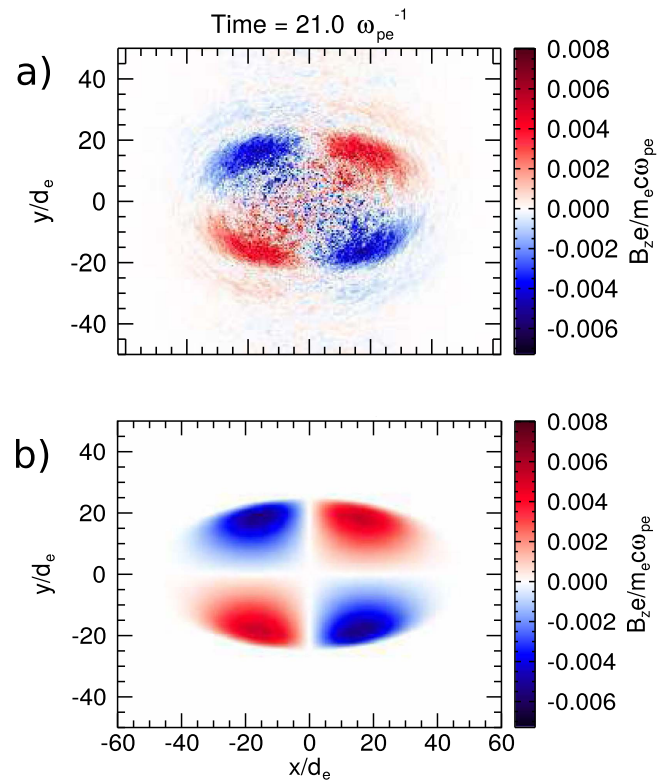


**Figure 4.** Out-of-plane magnetic field  $B_z$  generated by the Biermann battery from the PIC simulation (a) shown in figure 1 (from a simulation originally reported in [14], with  $L_T/d_e = 50$  ( $L_T/\lambda_D = 250$ ),  $m_i/m_e = 2000$ , at  $\omega_{pe}t = 21$ ). The predicted magnetic field (b) given by equation (25) for the initial density and temperature distribution from equation (58) shows agreement with the simulation results.

magnetic field ( $B_z$ ) is compared with the respective fields predicted in equation (25), for the initial density and temperature distribution from equation (58). Here, like in figure 1 we are looking at  $\omega_{pe}t = 21$ , which is much less than the crossing time  $\omega_{pe}t \sim \delta^{-1} = 250$ , so our assumptions are not largely broken. Although the linear predictions are not strictly accurate, again we find a good match with the fields from simulation.

## 7. Conclusions

We have performed kinetic calculations with density and temperature gradients, which predict the linear growth of magnetic fields, and the generation of a temperature anisotropy driven by the temperature gradient, in effectively collisionless regimes; this goes beyond the results from paper I [15] by allowing a completely general set of gradients. With this generality, a spatial dependent prediction of the temperature anisotropy (magnitude and direction) which coincides with the Weibel instabilities that this anisotropy drives, and the magnetic fields driven by the kinetic Biermann battery is now possible.

Similarly to the results reported in paper I [15], the kinetic outcome of the anisotropy generation is relevant even for some magnetized cases; as long as there are no gradients perpendicular to  $\mathbf{B}$ , where the magnetic field would affect the relevant particle motions. This phenomena is thus relevant for a wide variety of settings.

Likewise, for the more general case taken in this paper, the evolution of an anisotropic Maxwellian distribution ( $v_{Ti0} \neq v_{Tj0}$ , where  $v_{Ti0}$  is the thermal velocity in the  $i$  direction) can be modeled by the presented equations. In that case,  $\mathbf{x}$ ,  $\mathbf{v}$ , and  $\mathbf{E}$  are normalized using the  $v_{Ti0}$  in the same direction, and equation (25) has an additional factor of  $v_{Tx0}/v_{Ty0}$ . This reduces to the Biermann field being generated due to the thermal velocity solely in the direction of the density gradient.

## Acknowledgments

This work was supported by the European Research Council (ERC-2010-AdG Grant No. 267841, and ERC-2015-AdG Grant No. 695008).

## Appendix A. Distribution function of solution

The solution for the distribution function with arbitrary density and temperature gradients starting with no electromagnetic fields is

$$f = f_{\nabla n, \nabla T} + \tilde{f}_n + \tilde{f}_T + \tilde{f}_{n,T}, \quad (34)$$

while in the case with an initial equilibrium electric field:

$$\begin{aligned} \mathbf{E} = \mathbf{E}_{st} \equiv & -(\epsilon + \delta_{\parallel} - \epsilon^2 x + \kappa_{nix} \epsilon^2 x_i \\ & + \kappa_{Tix} \delta^2 x_i + \epsilon \delta_{\parallel} x + \epsilon \delta_{\perp} y) \hat{\mathbf{x}} \\ & - (\delta_{\perp} + \kappa_{niy} \epsilon^2 x_i + \kappa_{Tiy} \delta^2 x_i) \hat{\mathbf{y}} \\ & - (\kappa_{niz} \epsilon^2 x_i + \kappa_{Tiz} \delta^2 x_i) \hat{\mathbf{z}}, \end{aligned} \quad (35)$$

it is

$$f = f_{\nabla n, \nabla T}. \quad (36)$$

The term due to both a density and temperature gradient with the equilibrium field is:

$$\begin{aligned} f_{\nabla n, \nabla T} \equiv & f_{\nabla T} + \frac{1}{2} \epsilon (\delta_{\parallel} v_x + \delta_{\perp} v_y) \omega_{pe,x} t x (5 - v^2) f_M \\ & - \frac{1}{4} \epsilon \delta_{\parallel} (\omega_{pe,x} t)^2 (3 - v^2) f_M \\ & - \frac{1}{2} \epsilon \delta_{\parallel} (\omega_{pe,x} t)^2 (1 - v_x^2) f_M \\ & + \frac{1}{2} \epsilon \delta_{\perp} (\omega_{pe,x} t)^2 v_x v_y f_M, \end{aligned} \quad (37)$$

where the term due to just a temperature gradient with the equilibrium field is:

$$\begin{aligned} f_{\nabla T} \equiv & f_0 + \frac{1}{2} \delta \omega_{pe,x} t v_x' (5 - v^2) f_M \\ & - \frac{1}{4} \delta^2 \omega_{pe,x} t x' v_x' (25 - 12v^2 + v^4) f_M \\ & + \frac{1}{2} \delta^2 \kappa_{Tij} \omega_{pe,x} t x_i v_j (5 - v^2) f_M \\ & + \frac{1}{8} \delta^2 (\omega_{pe,x} t)^2 v_x'^2 (25 - 12v^2 + v^4) f_M \\ & + \frac{1}{4} \delta^2 (\omega_{pe,x} t)^2 [v_x'^2 (7 - v^2) - (5 - v^2)] f_M \\ & - \frac{1}{4} \delta^2 \kappa_{Tij} (\omega_{pe,x} t)^2 v_i v_j (5 - v^2) f_M, \end{aligned} \quad (38)$$

and the initial perturbed distribution function is:

$$\begin{aligned} f_0 = & f_M + \epsilon x f_M - \frac{1}{2} (\delta_{\parallel} x + \delta_{\perp} y) (3 - v^2) f_M \\ & + \frac{1}{2} \epsilon^2 \kappa_{nij} x_i x_j f_M - \frac{1}{4} \delta^2 \kappa_{Tij} x_i x_j (3 - v^2) f_M \\ & + \frac{1}{8} (\delta_{\parallel} x + \delta_{\perp} y)^2 (15 - 10v^2 + v^4) f_M \\ & - \frac{1}{2} \epsilon x (\delta_{\parallel} x + \delta_{\perp} y) (3 - v^2) f_M. \end{aligned} \quad (39)$$

The oscillatory term due to just a density gradient is:

$$\begin{aligned} \tilde{f}_n \equiv & -\epsilon \sin(\omega_{pe,x} t) v_x f_M \\ & - \epsilon^2 \kappa_{nij} \sin(\omega_{pe,x} t) x_j v_i f_M \\ & + \frac{1}{2} \epsilon^2 \sin(\omega_{pe,x} t) x v_x f_M \\ & + \epsilon^2 [1 - \cos(\omega_{pe,x} t)] (\kappa_{nij} v_i v_j - v_x^2) f_M \\ & + \frac{1}{2} \epsilon^2 t \sin(\omega_{pe,x} t) v_x^2 f_M \\ & - \frac{1}{2} \epsilon^2 [1 - \cos(\omega_{pe,x} t)]^2 (v_x^2 - 1) f_M, \end{aligned} \quad (40)$$

while the oscillatory term due to just a temperature gradient is:

$$\begin{aligned} \tilde{f}_T \equiv & -\delta \sin(\omega_{pe,x} t) v_x' f_M \\ & + \frac{1}{2} \delta^2 \sin(\omega_{pe,x} t) x' v_x' (5 - v^2) f_M \\ & - \delta^2 \kappa_{Tij} \sin(\omega_{pe,x} t) x_j v_i f_M \\ & - \frac{1}{2} \delta^2 [1 - \cos(\omega_{pe,x} t)] v_x'^2 (5 - v^2) f_M \\ & + \frac{1}{2} \delta^2 [1 - \cos(\omega_{pe,x} t)] [v_x'^2 (7 - v^2) - (5 - v^2)] f_M \\ & - \frac{1}{2} \delta^2 \omega_{pe,x} t \sin(\omega_{pe,x} t) [v_x'^2 (7 - v^2) - (5 - v^2)] f_M \\ & + \frac{1}{2} \delta^2 [1 - \cos(\omega_{pe,x} t)]^2 (1 - v_x'^2) f_M \\ & + \delta^2 \kappa_{Tij} [1 - \cos(\omega_{pe,x} t)] v_i v_j f_M, \end{aligned} \quad (41)$$



and the oscillatory term due to both a density and temperature gradient is:

$$\begin{aligned}
 \tilde{f}_{n,T} \equiv & -\epsilon(\delta_{\parallel}x + \delta_{\perp}y)\sin(\omega_{pe,x}t)v_x f_M \\
 & - \frac{1}{2}\epsilon(\delta_{\parallel}v_x + \delta_{\perp}v_y)\sin(\omega_{pe,x}t)x f_M \\
 & + \frac{1}{2}\epsilon(\delta_{\parallel}x + \delta_{\perp}y)\sin(\omega_{pe,x}t)v_x(5 - v^2)f_M \\
 & + 2\epsilon(\delta_{\parallel}v_x + \delta_{\perp}v_y)[1 - \cos(\omega_{pe,x}t)]v_x f_M \\
 & - \frac{1}{2}\epsilon\delta_{\parallel}[1 - \cos(\omega_{pe,x}t)](5 - v^2)f_M \\
 & + \epsilon(\delta_{\parallel}v_x + \delta_{\perp}v_y)[1 - \cos(\omega_{pe,x}t)]^2 v_x f_M \\
 & - \epsilon\delta_{\parallel}[1 - \cos(\omega_{pe,x}t)]^2 f_M \\
 & - \frac{1}{2}\epsilon(\delta_{\parallel}v_x + \delta_{\perp}v_y)\omega_{pe,x}t \sin(\omega_{pe,x}t)v_x(7 - v^2)f_M \\
 & + \frac{1}{2}\epsilon\delta_{\parallel}\omega_{pe,x}t \sin(\omega_{pe,x}t)v_x^2 f_M \\
 & + \frac{1}{2}\epsilon\delta_{\parallel}\omega_{pe,x}t \sin(\omega_{pe,x}t)(5 - v^2)f_M.
 \end{aligned} \tag{42}$$

The third to last term on the rhs of equation (38), which grows as  $t^2$ , is associated with the temperature anisotropy, while the last term results in modifications to the temperature tensor due to second order gradients, and also contributes to the temperature anisotropy. The third and fourth terms of equation (37), modify the isotropic temperature ( $\text{Tr}(T_{ij})$ ), and the temperature in the  $\hat{x}$  direction ( $T_{xx}$ ), respectively. The last term is associated with the off-diagonal component of the temperature tensor ( $T_{xy}$ ), which enhances and rotates the magnitude and direction of the temperature anisotropy (defined in the frame that diagonalizes  $T_{ij}$ ).

## Appendix B. Arbitrary frame conversion

In order to calculate the anisotropy from equation (31) in an arbitrary frame the following transformations to the temperature aligned frame are provided below.

$$\kappa'_{xx} = \frac{\kappa_{xx} + \kappa_{yy}}{2} + (\kappa_{xx} - \kappa_{yy})\frac{\delta_x^2 - \delta_y^2}{2\delta^2} + \kappa_{xy}\frac{2\delta_x\delta_y}{\delta^2}, \tag{43}$$

$$\kappa'_{yy} = \frac{\kappa_{xx} + \kappa_{yy}}{2} - (\kappa_{xx} - \kappa_{yy})\frac{\delta_x^2 - \delta_y^2}{2\delta^2} - \kappa_{xy}\frac{2\delta_x\delta_y}{\delta^2}, \tag{44}$$

$$\kappa'_{xy} = \kappa_{xy}\frac{\delta_x^2 - \delta_y^2}{\delta^2} - (\kappa_{xx} - \kappa_{yy})\frac{\delta_x\delta_y}{\delta^2}, \tag{45}$$

$$\epsilon_{\perp} = -\epsilon_x\frac{\delta_y}{\delta} + \epsilon_y\frac{\delta_x}{\delta}, \tag{46}$$

$$\epsilon_{\parallel} = \epsilon_x\frac{\delta_x}{\delta} + \epsilon_y\frac{\delta_y}{\delta}, \tag{47}$$

where  $\delta_i$ ,  $\epsilon_i$ , and  $\kappa_{ij}$  are the gradients as shown in equations (4)–(6) in the  $i$  and  $j$  directions of the arbitrary frame. Therefore, for equation (32):

$$\Delta_{\parallel} = (\kappa_{xx} - \kappa_{yy})\frac{\delta_x^2 - \delta_y^2}{\delta^2} + \kappa_{xy}\frac{4\delta_x\delta_y}{\delta^2}, \tag{48}$$

$$\Delta_{\perp} = 2\kappa_{xy}\frac{\delta_x^2 - \delta_y^2}{\delta^2} - 2(\kappa_{xx} - \kappa_{yy})\frac{\delta_x\delta_y}{\delta^2}. \tag{49}$$

The angle angle of rotation to the direction of maximum temperature shown in equation (33),  $\theta'$ , is also modified in an arbitrary frame.

$$\theta = \theta' + \theta_{\delta}, \tag{50}$$

where  $\theta_{\delta}$  is the angle between the arbitrary frame and the frame aligned the temperature gradient (in which we can take advantage of equations (31) and (33)):

$$\theta_{\delta} = \tan^{-1}\left(\frac{\delta_y}{\delta_x}\right). \tag{51}$$

## Appendix C. Anisotropy calculation

Given a 2D temperature tensor in an arbitrary frame, the anisotropy can be calculated as:

$$A = \frac{2T_{\text{ani}}}{T_{\text{iso}} - T_{\text{ani}}}, \tag{52}$$

where,

$$T_{\text{ani}} = \frac{1}{2}((T_{xx} - T_{yy})^2 + 4T_{xy}^2)^{1/2}, \tag{53}$$

$$T_{\text{iso}} = \frac{T_{xx} + T_{yy}}{2}. \tag{54}$$

The angle between an arbitrary frame and the frame indicated by the double prime notation (see equation (29)), where we diagonalize the in-plane components of the temperature tensor  $T_{ij}$ , is:

$$\theta = \frac{1}{2}\tan^{-1}\left(\frac{T_{xx} - T_{yy}}{T_{xy}}\right) + \frac{\pi}{2}(1 - \Theta(T_{xx} - T_{yy})). \tag{55}$$

Alternatively, the anisotropy can be expressed in vector form to indicate the direction where the temperature is hottest, without calculating the angle.

$$A_x = A\left(\frac{T_{\text{ani}} + T_{xx} - T_{yy}}{2T_{\text{ani}}}\right)^{1/2}, \tag{56}$$

$$A_y = A\left(\frac{T_{\text{ani}} - T_{xx} + T_{yy}}{2T_{\text{ani}}}\right)^{1/2}\text{sign}(T_{xy}). \tag{57}$$

## Appendix D. Density and temperature distributions

The initial density and temperature distributions used in the simulations are the following:

$$n = \begin{cases} (n_0 - n_b)\cos(\pi r/2L_T)^2 + n_b, & \text{if } r < L_T, \\ n_b, & \text{otherwise,} \end{cases}$$

$$v_T = \begin{cases} (v_{T0} - v_{T0b})\cos(\pi|x|/2L_T)^2 + v_{T0b}, & \text{if } |x| < L_T, \\ v_{T0b}, & \text{otherwise,} \end{cases} \quad (58)$$

$$\text{where } r = \sqrt{x^2 + (L_T/L_{ny})^2},$$

and we take  $n_b = 0.1n_0$  and  $v_{T0b} = 0.05v_{T0}$ . For the Weibel simulation  $|x|$  is replaced with  $r$  in equation (58). Note that in [13] and [14], this was erroneously expressed as:

$$n = \begin{cases} (n_0 - n_b)\cos(\pi r/2L_T) + n_b, & \text{if } r < L_T, \\ n_b, & \text{otherwise,} \end{cases}$$

$$v_T = \begin{cases} (v_{T0} - v_{T0b})\cos(\pi|x|/2L_T) + v_{T0b}, & \text{if } |x| < L_T, \\ v_{T0b}, & \text{otherwise,} \end{cases} \quad (59)$$

where the square was omitted.

## References

- [1] Stamper J A, Papadopoulos K, Sudan R N, Dean S O and McLean E A 1971 *Phys. Rev. Lett.* **26** 1012
- [2] Li C K, Seguin F H, Frenje J A, Rygg J R, Petrasso R D, Town R P J, Landen O L, Knauer J P and Smalyuk V A 2007 *Phys. Rev. Lett.* **99** 055001
- [3] Gregori G *et al* 2012 *Nature* **481** 480
- [4] Gao L, Nilson P M, Igumenshchev I V, Haines M G, Froula D H, Betti R and Meyerhofer D D 2015 *Phys. Rev. Lett.* **114** 215003
- [5] Cecchetti C A *et al* 2009 *Phys. Plasmas* **16** 043102
- [6] Kulsrud R M and Anderson S W 1992 *Astrophys. J.* **396** 606
- [7] Kulsrud R M and Zweibel E G 2008 *Rep. Prog. Phys.* **71** 046901
- [8] Albertazzi B *et al* 2014 *Science* **346** 325
- [9] Marocchino A, Atzeni S and Schiavi A 2016 *Phys. Plasmas* **23** 122307
- [10] Meinecke J *et al* 2014 *Nat. Phys.* **10** 520
- [11] Biermann L 1950 *Z. Naturforsch.* **5a** 65
- [12] Graziani C, Tzeferacos P, Lee D, Lamb D Q, Weide K, Fatenejad M and Miller J 2016 *J. Phys.: Conf. Ser.* **719** 012018
- [13] Schoeffler K M, Loureiro N F, Fonseca R A and Silva L O 2014 *Phys. Rev. Lett.* **112** 175001
- [14] Schoeffler K M, Loureiro N F, Fonseca R A and Silva L O 2016 *Phys. Plasmas* **23** 056304
- [15] Schoeffler K M, Loureiro N F and Silva L O 2017 arXiv:1707.06069 [physics.plasm-ph]
- [16] Weibel E S 1959 *Phys. Rev.* **114** 18
- [17] Levinson A and Eichler D 1992 *Astrophys. J.* **387** 212
- [18] Gary S P and Li H 2000 *Astrophys. J.* **529** 1131
- [19] Lindstedt A 1882 *Abhandlungen der Königlich Preussischen Akademie der Wissenschaften* 31
- [20] Poincaré H 1957 *Les Méthodes Nouvelles de la Mécanique Céleste, II (1882)* (New York: Dover)
- [21] Parker E N 1958 *Phys. Rev.* **109** 1874
- [22] Fonseca R A *et al* 2002 *Lect. Notes Comput. Sci.* **2331** 342
- [23] Fonseca R A, Martins S F, Silva L O, Tonge J W, Tsung F S and Mori W B 2008 *Plasma Phys. Control Fusion* **50** 124034
- [24] Epperlein E M and Haines M G 1986 *Phys. Fluids* **29** 1029
- [25] Chew G F, Goldberger M L and Low F E 1956 *Proc. R. Soc. A* **236** 112